THE JOURNAL OF PHYSICAL CHEMISTRY Letters

pubs.acs.org/JPCL Letter

Real-Time Tunneling Dynamics through Adiabatic Potential Energy Surfaces Shaped by a Conical Intersection

Kyung Chul Woo and Sang Kyu Kim*

Cite This: J. Phys. Chem. Lett. 2020, 11, 6730−6736 Read Online

ACCESS | Metrics & More | Article Recommendations | Supporting Information

ABSTRACT: Dynamic shaping of the adiabatic tunneling barrier in the S−H bond extension coordinate of several ortho-substituted thiophenols has been found to be mediated by low-frequency out-of-plane vibrational modes, which are parallel to the coupling vector of the branching plane comprising the conical intersection. The S−H predissociation tunneling rate (k) measured when exciting to the S_1 zero-point level of 2-methoxythiophenol $(44\ \text{ps})^{-1}$ increases abruptly, to $k \approx (22\ \text{ps})^{-1}$, at the energy corresponding to excitation of the 152 cm^{-1} out-of-plane vibrational mode and then falls back to $k \approx (40\ \text{ps})^{-1}$ when the in-plane mode is excited at 282 cm^{-1}. Similar resonance-like peaks in plots of S_1 tunneling rate versus internal energy are observed when exciting the corresponding low-frequency out-of-plane modes in the S_1 states of 2-fluorothiophenol and 2-chlorothiophenol. This experiment provides clear-cut evidence for dynamical "shaping" of the lower-lying adiabatic potential energy surfaces by the higher-lying conical intersection seam, which dictates the multidimensional tunneling dynamics.

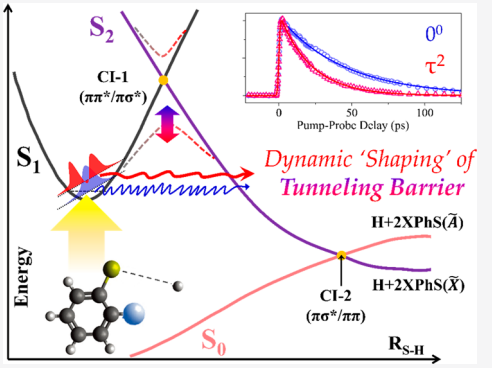

Structural properties of conical intersections and their influence on reaction dynamics are essential subjects that are indispensable for any thorough understanding and control of nonadiabatic transitions, which are ubiquitous in chemistry and biology.[1−4] For polyatomic molecules, the conical intersection on the two-dimensional branching plane is located on the $(3N - 8)$-dimensional seam, where N is the number of atoms. No conical intersection is unique. Rather, it is pictured as one of multiple conical intersections located on associated two-dimensional branching planes. Nonadiabatic transitions then take place most efficiently through these conical intersections. For instance, surface hopping from the upper to the lower adiabat is mediated by nuclear motion in the proximity of the conical intersection, where the Born−Oppenheimer approximation becomes invalid.[5,6] On the other hand, if the reactive flux or wavepacket involved in the particular reaction proceeds remote (in terms of structures and energetics) from the conical intersection, then the nuclear motion should be largely confined to one or the other adiabatic potential energy surface.[7−9] It should be emphasized that both upper and lower adiabatic potential surfaces are assumed to be dynamically shaped in the multidimensional coordinate space by the coupling nature of the conical intersection seam, especially in the vicinity of the region of surface crossing. In this regard, even when the reaction occurs mostly on a single adiabatic potential energy surface, these adiabatic surfaces are strongly modified by the topological shape of the conical intersection seam along multidimensional coordinates. Although there has been ample spectroscopic evidence,[10−14] few cases have been reported where the reaction dynamics are shown to be influenced by the "shaped" potential energy surfaces—especially for a tunneling process—although this situation has long been conceived theoretically and supported in part by some experimental evidence.[15−19] In this work, we demonstrate that tunneling rates are strongly influenced by potential energy surfaces whose topology is dynamically shaped by a higher-energy adiabatic potential energy surface in the vicinity of the conical intersection seam.

Herein, we investigate the hydrogen atom tunneling predissociation dynamics of three ortho-substituted thiophenols: 2-methoxythiophenol (2-MTP), 2-fluorothiophenol (2-FTP), and 2-chlorothiophenol (2-CTP). For thiophenols, the optically bright S_1 ($\pi\pi^*$) state is bound, whereas the higher-lying S_2 ($\pi\sigma^*$) state is repulsive along the S−H bond elongation coordinate, where the S_1 and S_2 labels denote the respective diabatic surfaces. The S−H bond predissociation then occurs by coupling of S_1 and S_2 as the two surfaces cross along the S−H bond elongation coordinate to give the S_1/S_2 conical intersection. And then, in the later stage of the reaction, the flux riding on the repulsive S_2 potential energy surface bifurcates to yield either the electronically excited $C_6H_5S\cdot$ radical ($\tilde{A}$) or the ground $C_6H_5S\cdot$ radical ($\tilde{X}$) at the S_0/S_2

Received: June 18, 2020
Accepted: July 27, 2020
Published: July 27, 2020

Downloaded via KOREA ADVANCED INST SCI AND TECHLGY on August 10, 2020 at 11:41:42 (UTC).
See https://pubs.acs.org/sharingguidelines for options on how to legitimately share published articles.

ACS Publications © XXXX American Chemical Society

conical intersection, as the S_2 or S_0 states correlate diabatically to, respectively, the $\tilde{X}$ or $\tilde{A}$ state radical (plus an H atom) at the asymptotic limit.[20−23] For thiophenol, its ultrashort excited state lifetime of ∼50 fs implies the S_1 potential energy surface is nearly repulsive due to the proximity of the S_1/S_2 conical intersection to the S_1 minimum structure, giving an extremely low tunneling barrier for the H atom detachment.[21,23,24] On the other hand, ortho-substituted thiophenols, which adopt only the *syn*-conformers in the jet-cooled environment, have much longer S_1 lifetimes, as evidenced by their well-resolved resonant-enhanced two-photon ionization (R2PI) spectra obtained with nanosecond laser excitation (cf., the complete absence of any nanosecond R2PI signal for bare thiophenol).[25−27] This already indicates that ortho-substituted thiophenols, due to the finite reaction barrier under their respective S_1/S_2 ($\pi\pi^*/\pi\sigma^*$) conical intersection seams, undergo classically forbidden hydrogen atom tunneling from the S_1 potential well. Here, we report S_1 vibronic state-specific lifetimes of 2-MTP, 2-FTP, and 2-CTP measured using a picosecond laser pump−probe scheme, along with appearance rates of the resulting H atom photofragments. Employing time-resolved velocity-map ion imaging methods, the growths of the product translational energy distributions have also been measured in real time. The tunneling rates are found to be strongly mode-dependent, which provides direct evidence of the "shaping" of the adiabatic potential energy surfaces by the higher-lying S_1/S_2 conical intersection seam.

The picosecond time-resolved parent ion transient measured following excitation to the S_1 origin of 2-MTP shows a single exponential decay with a lifetime of ∼44 ps, Figure 1. This is about 900 times longer than the 50 fs lifetime observed for bare thiophenol[24] but about 50 times shorter than the 2.3 ns lifetime measured for phenol.[28−33] Roughly, this indicates that the S_1 potential well of 2-MTP at its zero-point energy level is much deeper than that of thiophenol but is rather shallow compared to that of phenol.[25,26,34−38] It has been well-established that H atom tunneling largely determines the (rather long) S_1 lifetime found in the case of phenol.[29,30,39,40] Provided that the (nontunneling) contributions to nonradiative decay rate of 2-MTP are not much different to those in phenol, then the quantum yield of the H atom tunneling from 2-MTP must be close to unity. In other words, the much shorter (∼44 ps) S_1 lifetimes observed at the zero-point level of 2-MTP should be entirely attributable to the hydrogen atom tunneling rate. We have carried out rate measurements on the monodeuterated sample, 2-methoxythiophenol-d_1 (2-MTP-d_1). As Figure 1 shows, the primary isotope effect on the tunneling rate as a result of SH/SD substitution is huge, with measured lifetimes $\tau \approx 640$ or 410 ps when exciting at the S_1 origin and the τ_{OCH3}^2 (101 cm^{-1}) bands of 2-MTP-d_1, respectively. This more than an order of magnitude difference in the S_1 state lifetimes of 2-MPT and 2-MPT-d_1 confirms that S−H bond fission indeed involves a tunneling process.

As shown in the R2PI spectrum taken with the picosecond laser pulse ($\Delta E \approx 25$ cm^{-1}), Figure 1, each S_1-S_0 vibronic band of 2-MTP is well-isolated. Thus, the tunneling rate could be unambiguously measured for each S_1 vibronic level. The most dramatic experimental observation is that the tunneling rate is exceptionally strongly mode-dependent, particularly in the very low internal energy region. The tunneling rate increases approximately 2-fold when exciting the τ_{OCH3}^2 (101 cm^{-1}) or $10b^2$ (152 cm^{-1}) modes, giving corresponding lifetimes of ∼22 or 25 ps, respectively. Upon tuning to higher

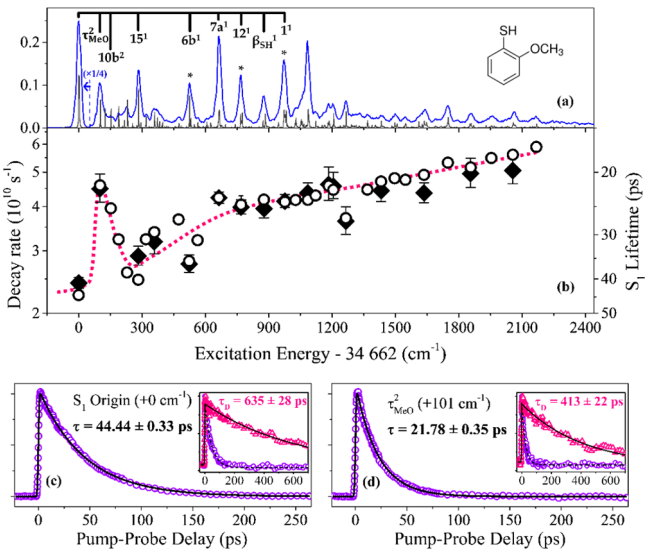

Figure 1. (a) Picosecond (1 + 1′) R2PI spectrum of 2-MTP (blue) overlaid with the nanosecond (1 + 1) R2PI spectrum (black) with the proper vibronic assignments.[27] Superposition of states coherently prepared within the picosecond laser pulse has been found at vibronic bands marked with asterisks, providing the precise frequency differences of doublets (see Supporting Information). (b) Plot of the tunneling rate constant (left ordinate) and S_1 lifetime (right ordinate) estimated from the transients of the parent ion (open circles) and the H^+ product (filled diamonds) signals. The red-dotted line is drawn to guide the eye. (c) The parent ion transient taken at the S_1 zero-point energy. For comparison, the corresponding transient of 2-MTP-d_1 (i.e., where the SH moiety has been substituted by SD) is shown in red in the inset. (d) The parent ion transient taken when exciting on the 101 cm^{-1} band with, again, the transient obtained when exciting the corresponding mode in 2-MTP-d_1 shown in red in the inset. For the full set of experimental data, see the Supporting Information. The Varsanyi notation was used for the mode description of all molecules here (for details, see the Supporting Information of ref 27. (Table S2)).

energy, the tunneling rate then quickly returns to values similar to that of the S_1 zero-point level, e.g., excitation on the 15^1 (282 cm^{-1}) band returns a lifetime $\tau \approx 40$ ps, Figure 1. Thereafter, the tunneling rate increases rather monotonically with increasing S_1 internal energy, though further fluctuations in lifetime are observed when exciting on several different vibronic modes.

Such huge fluctuations in tunneling rate within such a small energy range are very hard to explain without invoking the multidimensionality of the potential energy surfaces. For example, it is hard to conceive that the nuclear displacement vectors associated with the 101 or 152 cm^{-1} modes are coupled to the tunneling coordinate in any one-dimensional picture of the potential energy surface along the transition state well-defined as a saddle point on the top of the barrier. The 152 cm^{-1} mode, for instance, is assigned[27] to excitation of two quanta of the out-of-plane mode ($10b^2$), which involves the dihedral torsional motion of the S−H bond with respect to the molecular plane, Figure 2. Identifying and tracking multiple tunneling paths in multidimensional coordinates is nontrivial without far more detailed knowledge of the potential energy surfaces, including nonadiabatic couplings among multiple excited electronic configurations. Nevertheless, the present experimental observations strongly indicate that the tunneling potential energy surface is strongly perturbed by the higher-

https://dx.doi.org/10.1021/acs.jpclett.0c01892
J. Phys. Chem. Lett. 2020, 11, 6730−6736

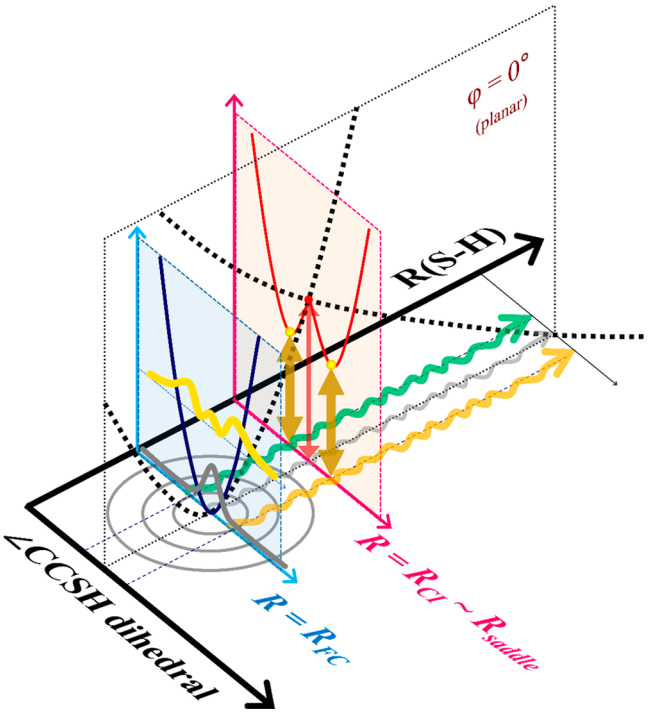

Figure 2. Schematic description of the two-dimensional potential energy surfaces along the S−H elongation (R(S−H)) and the CCSH dihedral angle coordinates. The tunneling path for reactive flux following excitation to the zero-point level at the Franck−Condon (FC) region ($R = R_{FC}$) experiences a reaction barrier, the top of which corresponds to the apex of the conical intersection (at $R = R_{CI} \approx R_{saddle}$), whereas out-of-plane motion allows the excited molecules to sample a lower effective barrier shaped by the higher-lying conical intersection.

lying conical intersection. Even though the gradient and coupling vectors constituting the branching plane cannot be fully replicated by a couple of S_1 parent normal modes, it is quite likely that the 10b mode is parallel to the coupling vector for the S_1/S_2 conical intersection (since one of the most influential coupling vectors for the S_1/S_2 conical intersection generated along the H atom tunneling path corresponds to the dihedral out-of-plane torsion of the S−H bond axis with respect to the molecular plane.[21,34,38])

In a two-dimensional picture involving the S−H bond elongation and out-of-plane torsional coordinates, the S_1/S_2 conical intersection appears as an apex at the planar geometry, with lower-lying saddle points[37,41] along the S−H out-of-plane torsional coordinate, Figure 2. Namely, the lower S_1 adiabatic potential energy surface, responsible for the finite S_1 lifetime due to the leakage of reactive flux by quantum tunneling through the barrier in the R(S−H) coordinate, is "shaped" by the upper-lying S_1/S_2 conical intersection. We note that the minimum energy geometry of 2-MTP in its S_1 state is pseudoplanar.[27] The reactive flux prepared when exciting the τ_{OCH3}^2 and/or $10b^2$ bands then should follow a path through a barrier that has been reduced by the associated out-of-plane coupling vectors at the conical intersection seam—facilitating H atom tunneling. The remarkable mode-dependent tunneling rate of 2-MTP, wherein large increases are observed upon exciting low-frequency out-of-plane mode excitations, is a direct consequence of the "shaping" of the multidimensional tunneling barrier mediated by the coupling vectors at the conical intersection seam.

The appearance rate of the H atom fragment, measured by the picosecond time-resolved pump−probe scheme, is found to be identical to the disappearance rate of the S_1 parent state, within the error limit. Translational energy distributions obtained from the time-resolved velocity-map ion images are all bimodal (see the Supporting Information). This bimodality has also been observed in previous studies on thiophenols and thioanisoles, and the interpretation is now firmly established. Namely, the deconvoluted peaks at lower and higher translational energies correspond to the reaction channels producing, respectively, $\tilde{A}$ or $\tilde{X}$ state 2-methoxy-PhS· radicals. The $\tilde{X}$ state radicals arise via nonadiabatic coupling at the S_0/S_2 conical intersection, whereas the $\tilde{A}$ state products result from reactive flux that follows the adiabatic path on the repulsive S_2 potential. Detailed analysis of the $\tilde{X}/\tilde{A}$ product branching ratio for 2-MTP-d_1 has been previously reported.[27] Geometric phase effects have been invoked as a potential explanation for activity in out-of-plane modes of the final fragment. Indeed, the tunneling paths under the potential energy surface near the saddle points around the apex of the conical intersection might lead to quantum interference between fluxes encircling with opposite directions, though tunneling paths are seemingly quite remote from the conical intersection.[42] As far as the tunneling rate is concerned, however, it is not straightforward to identify experimental signatures of geometrical phase effects from the present work alone.

The picosecond time-resolved parent ion transient following excitation to the S_1 origin of 2-FTP also shows a single exponential decay, with the lifetime of 12.3 ps, Figure 3. As in

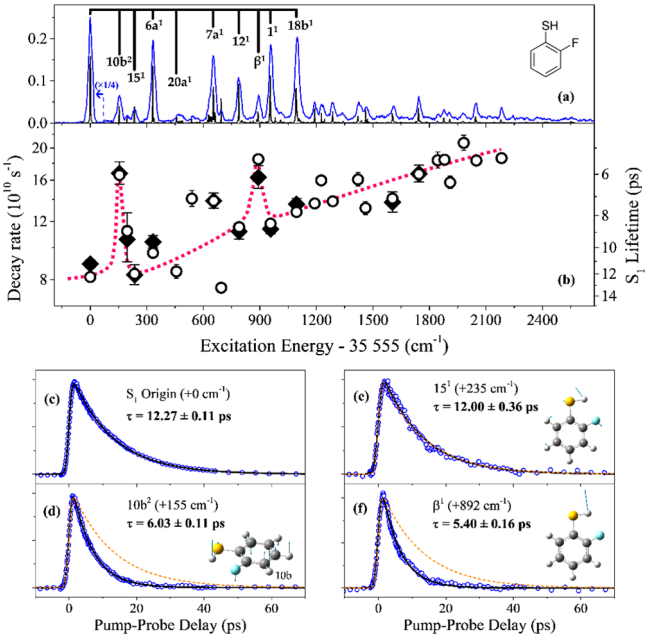

Figure 3. (a) Picosecond (1 + 1′) R2PI spectrum of 2-FTP (blue) overlaid with the nanosecond (1 + 1) R2PI spectrum (black) with vibronic assignments.[25] (b) Plot of the tunneling rate constant (left ordinate) and S_1 lifetime (right ordinate) estimated from the transients of the parent ion (open circles) and the H^+ product (filled diamonds). The red-dotted line is simply intended to guide the eye. (c−f) Parent transients taken at selected S_1 vibronic bands. The transients in (d−f) are compared with the ion transient taken at the S_1 zero-point level (dashed line). For the full set of experimental data, see Supporting Information.

https://dx.doi.org/10.1021/acs.jpclett.0c01892
J. Phys. Chem. Lett. 2020, 11, 6730−6736

the case of 2-MTP, the S_1 lifetime is reduced, to $\tau \approx 6.0$ ps (i.e., by roughly a factor of 2), when exciting the lowest-frequency vibronic band at 155 cm^{-1} and then increases again (to $\tau \approx 12$ ps) when exciting the 235 cm^{-1} mode. The 155 cm^{-1} feature corresponds to exciting two quanta of the out-of-plane mode ($10b^2$) involving dihedral torsional motion of the S−H bond relative to the molecular plane, whereas the 235 cm^{-1} band is associated with the in-plane 15^1 mode.[4,27] Thereafter, the tunneling rate increases rather monotonically with increasing S_1 internal energy although, again, significant mode-dependent fluctuations in lifetime are observed.

We note that excitation of the β (~892 cm^{-1}) mode associated with in-plane S−H bending motion[26] also expedites the S−H tunneling rate in 2-FTP in a mode-specific way, Figure 3. The rate enhancement (~1.4 times compared to those measured when exciting adjacent modes) is less dramatic than in the case of 155 cm^{-1} excitation. Again, however, the increase of the tunneling rate upon β mode excitation could be attributed to its coupling to the tunneling reaction coordinate, as the tunneling is not necessarily confined to the one-dimensional S−H stretching motion. This finding may imply that the S−H bending mode is parallel to the gradient vector of the conical intersection, which would be consistent with previous experimental findings that the conical intersection seam in the S_1 state predissociation of thiophenol-d_1 is accessed by the SD bending mode excitation.[23] Of the molecules studied here, the mode-dependent fluctuations in tunneling rate seem most pronounced in the case of 2-FTP. Recalling Figure 3, we see that the tunneling rates when exciting at 539 cm^{-1} ($15^1 6a^1$) and at 655 cm^{-1} ($7a^1$) are both faster than the smooth monotonic trend. As described earlier, the mode-specific fluctuation of tunneling rates continues up to an S_1 internal energy of ~1000 cm^{-1}. At yet higher energies, the tunneling rate increases monotonically, implying that the rate of intramolecular vibrational redistribution (IVR) is comparable to, or exceeds, the tunneling rate.

The variation in 2-CTP S_1 state lifetime with increasing internal energy is somewhat different to that found for 2-FTP and 2-MTP. The lifetime of the S_1 origin is measured to be ~227 ps, Figure 4. This lifetime is, respectively, ~5 and ~20 times longer than that of 2-MTP and 2-FTP (*vide supra*). The rapid increase in tunneling rate with increasing internal energy is also observed in 2-CTP. Excitation of the out-of-plane mode at 195 cm^{-1} gives a much-reduced lifetime (~104 ps), but the tunneling rate then slows again, giving $\tau \approx 197$ ps when exciting the 301 cm^{-1} band. Thereafter, the S_1 lifetime decreases rapidly with increasing internal energy. For instance, the S_1 lifetime of 2-CTP is only ~60 ps at ~600 cm^{-1} and has declined to ~11 ps at ~1100 cm^{-1}, Figure 4. Such a rapid increase in the S_1 dephasing rate cannot be explained solely by a tunneling process but rather suggests that a new, fast, nonradiative decay channel opens for 2-CTP at quite low internal energies, which rapidly overwhelms the (relatively slow) H atom tunneling process. Nonradiative transitions such as internal conversion and/or intersystem crossing leading to HCl product formation[43,44] might be responsible for this new channel. The S_1 dephasing mechanism of 2-CTP has not yet been resolved, and further investigations would be desirable.

The tunneling process can be pictured semiclassically as repeated attempts by the H atom to escape from the S_1 potential well, with some finite leakage probability. In such a picture, the tunneling probability is proportional to the S−H bond stretching frequency and inversely proportional to the

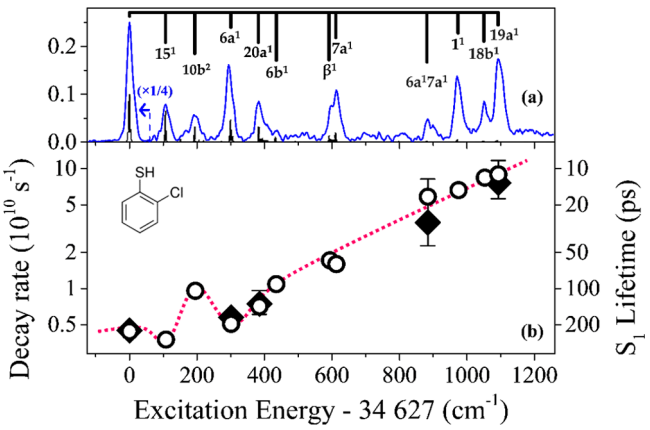

Figure 4. (a) Picosecond (1 + 1′) R2PI spectrum of 2-CTP (blue) overlaid with the nanosecond (1 + 1) R2PI spectrum (black) with vibronic assignments.[25] (b) Plot of the tunneling rate constant (left ordinate) and S_1 lifetime (right ordinate) estimated from the transients of the parent ion (open circles) and the H^+ product (filled diamonds). The red-dotted line is intended simply to help guide the eye. For the full set of experimental data, see the Supporting Information.

area of the adiabatic potential energy curve above the tunneling path. Such a simple one-dimensional, semiclassical picture would suggest that the tunneling rate would be rather insensitive by excitation of a low-frequency vibrational mode orthogonal to the S−H tunneling coordinate. In reality, however, one should recognize multiple tunneling paths in a multidimensional coordinate space. In the two-dimensional picture shown in Figure 2, the shortest tunneling path will be strongly dependent on the quantum mechanical nature of the initially prepared reactive flux. For the S_1 zero-point level, for instance, the reactive flux will be localized at the center of the S_1 potential well with respect to both the R(S−H) stretch and torsion coordinates. The shortest tunneling path starting from this localized geometry would sample the maximum tunneling barrier height set by the apex of the conical intersection (though it is not strictly forbidden for the tunneling to occur via some lower-energy paths below the saddle points set by the S−H bond torsional coupling vector due to the nature of quantum uncertainty). Given the topology of the S_1 potential well, there is little torque on the S−H bond, and it is less likely that reactive flux at the zero-point level experiences any significant distortion along the out-of-plane torsional coordinate. In this respect, the tunneling paths from the zero-point level should be limited to lying within only a small dihedral angle region—as depicted by the gray arrow in Figure 2. Conversely, flux prepared with out-of-plane mode excitation can sample tunneling paths distributed over a much wider range of dihedral torsional angles (yellow and green arrows in Figure 2). Assuming that the nuclear motion is not affected directly by the shape of the upper-lying potential energy surface (at least during the tunneling process), the tunneling path for molecules with torsional mode excitation will involve passage through a barrier whose height has been significantly lowered by the nonadiabatic coupling at the conical intersection. Flux prepared by exciting the out-of-plane mode would be able to tunnel through a barrier, the top of which is near the local saddle point generated by the negative gradient of the conical intersection along the coupling vector.

https://dx.doi.org/10.1021/acs.jpclett.0c01892
J. Phys. Chem. Lett. 2020, 11, 6730−6736

This picture, though not quantitative, succeeds in explaining why such a small energy increment can cause such a dramatic increase in tunneling rate. The explanation is reinforced by the fact that the tunneling rates in all three ortho-substituted thiophenols return to values similar to those observed at the respective S_1 origins when exciting adjacent in-plane modes, Figures 1, 3, and 4. This experimental finding strongly supports the view that the resonance-like peaks in the plots of tunneling rate versus internal energy found when exciting the low-frequency out-of-plane modes reflect the much enhanced tunneling efficiency of the reaction paths under the saddle points of the S_1 adiabatic potential energy surface along the out-of-plane torsion coordinate.

For calculating absolute tunneling rates, however, theory has shown the need for proper inclusion of geometric phase effects arising from the presence of the conical intersection.[18] Namely, the tunneling reaction occurring under the conical intersection is nonadiabatic in nature, and its dynamics is thus sensitive to the geometric phase as the reactive flux traverses around the conical intersection. Thereafter, constructive and/or destructive interference of the emerging flux (wavepacket) may lead to potentially dramatic mode-dependent tunneling rates. In this regard, state-of-the-art theoretical treatments on suitable high-dimensionality potential energy surfaces would be highly desirable. Comparing to the more extensively studied case of phenol,[32,33] the H atom tunneling rates following excitation to the origin levels of the S_1 states of 2-MTP, 2-FTP, and 2-CTP are found to be, respectively, ∼50, ∼150, and ∼10 times faster (*vide supra*). Though the detailed dynamics of phenol and the ortho-substituted thiophenols are likely to be quite different, it can be fairly stated that the energetic location of the S_1/S_2 conical intersection is much closer to the S_1 minimum in 2-MTP, 2-FTP, or 2-CTP than in the case of phenol. Thus, the dynamic influences of the higher-lying conical intersection on the tunneling dynamics in 2-MTP, 2-FTP, or 2-CTP can be expected to be larger and more evident in terms of the shaping of the lower and upper adiabatic potential energy surfaces, their multidimensionality, the geometrical phase effect, and/or the nonadiabatic coupling strengths. The present experimental results should provide a very good platform for a much better understanding of tunneling dynamics in the proximity of a conical intersection.

In summary, we have demonstrated that the S−H bond predissociation reactions of 2-methoxythiophenol, 2-fluorothiophenol, and 2-chlorothiophenol involve quantum-mechanical tunneling through adiabatic potential energy barriers that have been dynamically "shaped" by the higher-lying conical intersection seam. The observation of resonance-like peaks in the plots of tunneling rate versus internal energy, associated with very low-frequency out-of-plane vibrational motions, show that the dissociation is very sensitive to the dispersion of the reactive flux along out-of-plane coordinates parallel to the coupling vector comprising the conical intersection seam. The present study highlights the extreme sensitivity of the tunneling dynamics to the quantum-mechanical nature of the reactive flux and its vibrational energy content, shedding new light on the intimate relationship between molecular structure and chemical reactivity in polyatomic molecules.

EXPERIMENTAL METHODS

The experimental procedures for the results have been described elsewhere.[33,45,46] Briefly, neon carrier gas (2 bar pressure) was bubbled through the sample (heated to 50/60/60 °C for 2-fluorothiophenol, 2-methoxythiophenol, and 2-chlorothiophenol (all purchased from TCI Chemical), respectively) and expanded into vacuum through a nozzle operated by a 200 Hz pulsed Even−Lavie valve. The velocity-map imaging (VMI) electrodes were used to repel and accelerate parent and fragment ions through a 30 cm long time-of-flight region to the position-sensitive detector (PSD) equipped with Chevron-type microchannel plates (MCP) backed by a P46 phosphor screen. For the parent transients, the luminescence from the phosphor was collected by the photomultiplier tube (PMT, Hamamatsu) and monitored as a function of the pump−probe time delay. For the time-resolved ion images, a pulsed voltage gate was applied to the MCPs (DEI, PVX-4140) to select the ion of a specific mass-to-charge ratio. Ion spots on the phosphor screen were then captured by a triggered CMOS camera (PointGrey, GS3-U3-32S4) for each event. Each camera image was processed with an area threshold condition in order to avoid hot-pixel contribution and accumulated in the event-count mode and reconstructed three-dimensionally with the polar onion peeling (POP) method. Picosecond laser pulses were generated from the 1 kHz dual-synchronized ps/fs Ti:sapphire regenerative amplifier systems seeded with a single fs oscillator. Tunable UV frequencies for pump/probe wavelengths were obtained by nonlinear mixing of pulses from optical parametric amplifier (OPA) units pumped by split fundamental outputs from the picosecond regenerative amplifier system. Pump and probe laser pulses were nearly collinearly aligned and focused onto the gas mixture in the pulsed supersonic jet with the plano-convex spherical lenses (f = 300 mm) through a 1 mm thick ultraviolet fused silica window. Further experimental details are given in the Supporting Information.

ASSOCIATED CONTENT

Supporting Information

The Supporting Information is available free of charge at https://pubs.acs.org/doi/10.1021/acs.jpclett.0c01892.

Experimental details; tunneling rates at the S_1 origins; mode-specific lifetimes; experimental quantification of multidimensional tunnelling barriers; transients and time-resolved product state distributions of 2-fluorothiophenol, 2-methoxythiophenol, and 2-chlorothiophenol (PDF)

AUTHOR INFORMATION

Corresponding Author

Sang Kyu Kim − *Department of Chemistry, KAIST, Daejeon 34141, Republic of Korea;* orcid.org/0000-0003-4803-1327; Email: sangkyukim@kaist.ac.kr

Author

Kyung Chul Woo − *Department of Chemistry, KAIST, Daejeon 34141, Republic of Korea;* orcid.org/0000-0002-9387-9397

Complete contact information is available at: https://pubs.acs.org/10.1021/acs.jpclett.0c01892

Notes

The authors declare no competing financial interest.

https://dx.doi.org/10.1021/acs.jpclett.0c01892
J. Phys. Chem. Lett. 2020, 11, 6730−6736

■ ACKNOWLEDGMENTS

We appreciate the very helpful discussion with Prof. Mike Ashfold at the University of Bristol. We appreciate Mr. Do Hyung Kang for his experimental assistance. This work was financially supported by the National Research Foundation under the Project Numbers: 2018R1A2B3004534 and 2019R1A6A1A10073887.

■ REFERENCES

(1) Polli, D.; Altoe, P.; Weingart, O.; Spillane, K. M.; Manzoni, C.; Brida, D.; Tomasello, G.; Orlandi, G.; Kukura, P.; Mathies, R. A.; Garavelli, M.; Cerullo, G. Conical intersection dynamics of the primary photoisomerization event in vision. *Nature* **2010**, *467* (7314), 440−3.

(2) Deb, S.; Weber, P. M. The ultrafast pathway of photon-induced electrocyclic ring-opening reactions: the case of 1,3-cyclohexadiene. *Annu. Rev. Phys. Chem.* **2011**, *62* (1), 19−39.

(3) Musser, A. J.; Liebel, M.; Schnedermann, C.; Wende, T.; Kehoe, T. B.; Rao, A.; Kukura, P. Evidence for conical intersection dynamics mediating ultrafast singlet exciton fission. *Nat. Phys.* **2015**, *11* (4), 352−357.

(4) You, H. S.; Han, S.; Yoon, J.-H.; Lim, J. S.; Lee, J.; Kim, S.-Y.; Ahn, D.-S.; Lim, J. S.; Kim, S. K. Structure and dynamic role of conical intersections in the $\pi\sigma^*$-mediated photodissociation reactions. *Int. Rev. Phys. Chem.* **2015**, *34* (3), 429−459.

(5) Tully, J. C. Perspective: Nonadiabatic dynamics theory. *J. Chem. Phys.* **2012**, *137* (22), 22A301.

(6) Domcke, W.; Yarkony, D. R. Role of conical intersections in molecular spectroscopy and photoinduced chemical dynamics. *Annu. Rev. Phys. Chem.* **2012**, *63* (1), 325−52.

(7) Xie, C.; Malbon, C. L.; Yarkony, D. R.; Xie, D.; Guo, H. Signatures of a Conical Intersection in Adiabatic Dissociation on the Ground Electronic State. *J. Am. Chem. Soc.* **2018**, *140* (6), 1986−1989.

(8) Liu, F.; Beames, J. M.; Petit, A. S.; McCoy, A. B.; Lester, M. I. Infrared-driven unimolecular reaction of CH_3CHOO Criegee intermediates to OH radical products. *Science* **2014**, *345* (6204), 1596−1598.

(9) Lovejoy, E. R.; Kim, S. K.; Moore, C. B. Observation of Transition-State Vibrational Thresholds in the Rate of Dissociation of Ketene. *Science* **1992**, *256* (5063), 1541−1544.

(10) Cederbaum, L. S.; Friedman, R. S.; Ryaboy, V. M.; Moiseyev, N. Conical intersections and bound molecular states embedded in the continuum. *Phys. Rev. Lett.* **2003**, *90* (1), 013001.

(11) Schuurman, M. S.; Weinberg, D. E.; Yarkony, D. R. On the simulation of photoelectron spectra in molecules with conical intersections and spin-orbit coupling: The vibronic spectrum of CH_3S. *J. Chem. Phys.* **2007**, *127* (10), 104309.

(12) Schulenburg, A. M.; Merkt, F. Rotationally resolved photoelectron spectroscopic study of the Jahn−Teller effect in allene. *J. Chem. Phys.* **2009**, *130* (3), 034308.

(13) Ahn, D. S.; Kim, S. Y.; Lim, G. I.; Lee, S.; Choi, Y. S.; Kim, S. K. Mode-dependent Fano resonances observed in the predissociation of diazirine in the S_1 state. *Angew. Chem., Int. Ed.* **2010**, *49* (7), 1244−7.

(14) Han, S.; Lim, J. S.; Yoon, J. H.; Lee, J.; Kim, S. Y.; Kim, S. K. Conical intersection seam and bound resonances embedded in continuum observed in the photodissociation of thioanisole-d_3. *J. Chem. Phys.* **2014**, *140* (5), 054307.

(15) Vieuxmaire, O. P.; Lan, Z.; Sobolewski, A. L.; Domcke, W. *Ab initio* characterization of the conical intersections involved in the photochemistry of phenol. *J. Chem. Phys.* **2008**, *129* (22), 224307.

(16) Weiler, M.; Miyazaki, M.; Feraud, G.; Ishiuchi, S.; Dedonder, C.; Jouvet, C.; Fujii, M. Unusual Behavior in the First Excited State Lifetime of Catechol. *J. Phys. Chem. Lett.* **2013**, *4* (22), 3819−3823.

(17) Capello, M. C.; Broquier, M.; Ishiuchi, S.; Sohn, W. Y.; Fujii, M.; Dedonder-Lardeux, C.; Jouvet, C.; Pino, G. A. Fast nonradiative decay in *o*-aminophenol. *J. Phys. Chem. A* **2014**, *118* (11), 2056−62.

(18) Xie, C.; Ma, J.; Zhu, X.; Yarkony, D. R.; Xie, D.; Guo, H. Nonadiabatic Tunneling in Photodissociation of Phenol. *J. Am. Chem. Soc.* **2016**, *138* (25), 7828−7831.

(19) Ashfold, M. N. R.; Bennett, C. L.; Dixon, R. N. Predissociation dynamics of Ã-state ammonia probed by two-photon excitation spectroscopy. *Chem. Phys.* **1985**, *93* (2), 293−306.

(20) Lim, I. S.; Lim, J. S.; Lee, Y. S.; Kim, S. K. Experimental and theoretical study of the photodissociation reaction of thiophenol at 243 nm: Intramolecular orbital alignment of the phenylthiyl radical. *J. Chem. Phys.* **2007**, *126* (3), 034306.

(21) Devine, A. L.; Nix, M. G. D.; Dixon, R. N.; Ashfold, M. N. R. Near-Ultraviolet Photodissociation of Thiophenol. *J. Phys. Chem. A* **2008**, *112* (39), 9563−9574.

(22) Lim, J. S.; Choi, H.; Lim, I. S.; Park, S. B.; Lee, Y. S.; Kim, S. K. Photodissociation Dynamics of Thiophenol-d_1: The Nature of Excited Electronic States along the S-D Bond Dissociation Coordinate. *J. Phys. Chem. A* **2009**, *113* (39), 10410−10416.

(23) You, H. S.; Han, S.; Lim, J. S.; Kim, S. K. ($\pi\pi^*/\pi\sigma^*$) Conical Intersection Seam Experimentally Observed in the S−D Bond Dissociation Reaction of Thiophenol-d_1. *J. Phys. Chem. Lett.* **2015**, *6* (16), 3202−3208.

(24) Ovejas, V.; Fernández-Fernández, M.; Montero, R.; Longarte, A. On the ultrashort lifetime of electronically excited thiophenol. *Chem. Phys. Lett.* **2016**, *661*, 206−209.

(25) Han, S.; You, H. S.; Kim, S.-Y.; Kim, S. K. Dynamic role of the intramolecular hydrogen bonding in nonadiabatic chemistry revealed in the UV photodissociation reactions of 2-fluorothiophenol and 2-chlorothiophenol. *J. Phys. Chem. A* **2014**, *118* (34), 6940−9.

(26) Marchetti, B.; Karsili, T. N. V.; Cipriani, M.; Hansen, C. S.; Ashfold, M. N. R. The near ultraviolet photodissociation dynamics of 2- and 3-substituted thiophenols: Geometric *vs.* electronic structure effects. *J. Chem. Phys.* **2017**, *147* (1), 013923.

(27) Lim, J. S.; You, H. S.; Kim, S.-Y.; Kim, J.; Park, Y. C.; Kim, S. K. Vibronic structure and predissociation dynamics of 2-methoxythiophenol (S_1): The effect of intramolecular hydrogen bonding on nonadiabatic dynamics. *J. Chem. Phys.* **2019**, *151* (24), 244305.

(28) Berden, G.; Meerts, W. L.; Schmitt, M.; Kleinermanns, K. High resolution UV spectroscopy of phenol and the hydrogen bonded phenol-water cluster. *J. Chem. Phys.* **1996**, *104* (3), 972−982.

(29) Ratzer, C.; Küpper, J.; Spangenberg, D.; Schmitt, M. The structure of phenol in the S_1-state determined by high resolution UV-spectroscopy. *Chem. Phys.* **2002**, *283* (1−2), 153−169.

(30) Pino, G. A.; Oldani, A. N.; Marceca, E.; Fujii, M.; Ishiuchi, S.-I.; Miyazaki, M.; Broquier, M.; Dedonder, C.; Jouvet, C. Excited state hydrogen transfer dynamics in substituted phenols and their complexes with ammonia: $\pi\pi^*$-$\pi\sigma^*$ energy gap propensity and *ortho*-substitution effect. *J. Chem. Phys.* **2010**, *133* (12), 124313.

(31) Roberts, G. M.; Chatterley, A. S.; Young, J. D.; Stavros, V. G. Direct Observation of Hydrogen Tunneling Dynamics in Photoexcited Phenol. *J. Phys. Chem. Lett.* **2012**, *3* (3), 348−352.

(32) Lai, H. Y.; Jhang, W. R.; Tseng, C.-M. Communication: Mode-dependent excited-state lifetime of phenol under the S_1/S_2 conical intersection. *J. Chem. Phys.* **2018**, *149* (3), 031104.

(33) Woo, K. C.; Kim, S. K. Multidimensional H Atom Tunneling Dynamics of Phenol: Interplay between Vibrations and Tunneling. *J. Phys. Chem. A* **2019**, *123* (8), 1529−1537.

(34) Venkatesan, T. S.; Ramesh, S. G.; Lan, Z.; Domcke, W. Theoretical analysis of photoinduced H-atom elimination in thiophenol. *J. Chem. Phys.* **2012**, *136* (17), 174312.

(35) An, H.; Choi, H.; Lee, Y. S.; Baeck, K. K. Factors Affecting the Branching Ratio of Photodissociation: Thiophenol Studied through Quantum Wavepacket Dynamics. *ChemPhysChem* **2015**, *16* (7), 1529−34.

(36) Lin, G. S.; Xie, C.; Xie, D. Three-Dimensional Diabatic Potential Energy Surfaces for the Photodissociation of Thiophenol. *J. Phys. Chem. A* **2017**, *121* (44), 8432−8439.

(37) Zhang, L.; Truhlar, D. G.; Sun, S. Electronic spectrum and characterization of diabatic potential energy surfaces for thiophenol. *Phys. Chem. Chem. Phys.* **2018**, *20* (44), 28144−28154.

https://dx.doi.org/10.1021/acs.jpclett.0c01892
J. Phys. Chem. Lett. 2020, 11, 6730−6736

(38) Zhang, L.; Truhlar, D. G.; Sun, S. Full-dimensional three-state potential energy surfaces and state couplings for photodissociation of thiophenol. *J. Chem. Phys.* **2019**, *151* (15), 154306.
(39) Lipert, R. J.; Bermudez, G.; Colson, S. D. Pathways of S_1 decay in phenol, indoles, and water complexes of phenol and indole in a free jet expansion. *J. Phys. Chem.* **1988**, *92* (13), 3801−3805.
(40) Sobolewski, A. L.; Domcke, W.; Dedonder-Lardeux, C.; Jouvet, C. Excited-state hydrogen detachment and hydrogen transfer driven by repulsive $^1\pi\sigma^*$ states: A new paradigm for nonradiative decay in aromatic biomolecules. *Phys. Chem. Chem. Phys.* **2002**, *4* (7), 1093−1100.
(41) Xu, X.; Zheng, J.; Yang, K. R.; Truhlar, D. G. Photodissociation dynamics of phenol: multistate trajectory simulations including tunneling. *J. Am. Chem. Soc.* **2014**, *136* (46), 16378−86.
(42) Nix, M. G. D.; Devine, A. L.; Dixon, R. N.; Ashfold, M. N. R. Observation of geometric phase effect induced photodissociation dynamics in phenol. *Chem. Phys. Lett.* **2008**, *463* (4−6), 305−308.
(43) Yamamoto, S.; Ebata, T.; Ito, M. Rotational isomers of *o*-chlorophenol and their different emission properties. *J. Phys. Chem.* **1989**, *93* (17), 6340−6345.
(44) Harris, S. J.; Karsili, T. N.V.; Murdock, D.; Oliver, T. A. A.; Wenge, A. M.; Zaouris, D. K.; Ashfold, M. N. R.; Harvey, J. N.; Few, J. D.; Gowrie, S.; Hancock, G.; Hadden, D. J.; Roberts, G. M.; Stavros, V. G.; Spighi, G.; Poisson, L.; Soep, B. A Multipronged Comparative Study of the Ultraviolet Photochemistry of 2-, 3-, and 4-Chlorophenol in the Gas Phase. *J. Phys. Chem. A* **2015**, *119* (23), 6045−56.
(45) Woo, K. C.; Kang, D. H.; Kim, S. K. Real-Time Observation of Nonadiabatic Bifurcation Dynamics at a Conical Intersection. *J. Am. Chem. Soc.* **2017**, *139* (47), 17152−17158.
(46) Woo, K. C.; Kim, S. K. Mode-specific Excited-state Dynamics of *N*-Methylpyrrole. *Phys. Chem. Chem. Phys.* **2019**, *21* (26), 14387−14393.

https://dx.doi.org/10.1021/acs.jpclett.0c01892
J. Phys. Chem. Lett. 2020, 11, 6730−6736